ELSEVIER

Journal of Alloys and Compounds 239 (1996) 183–192

Journal of
ALLOYS
AND COMPOUNDS

Sputtered decorative hard coatings within the system LaB_6–ZrB_2

C. Mitterer[a], H.-M. Ott[a,1], J. Komenda-Stallmaier[a,2], P. Schmölz[b], W.S.M. Werner[b], H. Störi[b]

[a]*Institut für Metallkunde und Werkstoffprüfung, Montanuniversität, Franz-Josef-Straße 18, A-8700 Leoben, Austria*
[b]*Institut für Allgemeine Physik, Technische Universität, Wiedner Hauptstraße 8-10, A-1040 Wien, Austria*

Received 2 November 1995; in final form 12 December 1995

Abstract

Decorative coatings have to meet a variety of requirements such as attractive colour as well as high wear and corrosion resistance. Within this work, coatings were deposited onto steel and molybdenum substrates by non-reactive magnetron sputtering using various targets within the quasi-binary eutectic section LaB_6–ZrB_2 with the goal to improve the mechanical properties of violet coloured LaB_6-based coatings. Coating characterization was done using scanning electron microscopy, electron-probe microanalysis, X-ray diffraction, Vickers microhardness measurements and CIE-$L^*a^*b^*$ colorimetry. For sputtering from both compounds of the section LaB_6–ZrB_2, violet and silver-grey crystalline films with high hardness values were respectively obtained. For the ZrB_2 target contents investigated within the two-phase region of the equilibrium diagram (25, 55, and 75 at.% ZrB_2), coatings showed a pronounced tendency to form partially or fully amorphous structures. These structures were accompanied by low hardness values and a silver-grey appearance. Although being unsuccessful with optimization of both mechanical and optical properties of ZrB_2-alloyed LaB_6-based coatings, complex hard coatings have a substantial development potential in various application fields.

Keywords: Decorative coatings; PVD; Magnetron sputtering; Borides

1. Introduction

Owing to their low work function for thermionic emission [1] and their blue to red colorations [2,3] the hexaborides of the rare-earth metals are potential candidates for the application as thin coatings on filaments [4–6] as well as for decorative purposes [7,8]. Several approaches to deposit coatings mainly based on the purple-red lanthanum hexaboride LaB_6 are reported in the literature and include electrophoretic deposition [9,10] as well as PVD techniques [4–8,11–13]. Although reasonable results have been obtained, most of the films deposited seem to suffer from high stresses and porosity as well as low adhesion limiting their applicability. These drawbacks may be related to the crystal structure of these compounds. The rare-earth hexaborides form a crystal lattice in which the rare-earth atoms and boron octahedra are arranged in the same manner as the Cl^- and Cs^+ ions in the CsCl structure type [14]. The structure of the hexaborides is dominated by strong B–B bonds allowing wide composition ranges without significant deviations from the lattice parameter. For example, the B/La atomic ratio for LaB_6 may vary between 6 and 7.8 [15]; these deviations from stoichiometry are accommodated by the formation of lanthanum vacancies.

Some of the drawbacks arising from the distinct atomic binding structure of LaB_6 may be overcome by alloying with suitable elements or compounds. For thermodynamic reasons it is impossible to select a suitable transition metal for the development of LaB_6–Me coatings. The main emphasis of this investigation is laid on sputtered coatings within the system LaB_6–ZrB_2. This quasi-binary section of the ternary La–Zr–B system shows a simple eutectic with the eutectic point at 31 at.% ZrB_2 and 2470°C [16]. The maximum solubilities for the second component are less than 3 at.%, resulting in a wide-range two-

[1] Present address: Materialprüfanstalt der Österreichischen Bundesbahn, Landgutgasse 28, A-1100 Wien, Austria.
[2] Present address: Merten International, Hauptstraße 13, A-2333 Leopoldsdorf, Austria.

0925-8388/96/$15.00 © 1996 Elsevier Science S.A. All rights reserved
PII S0925-8388(96)02214-1

phase region. Alloys within this system have shown promising thermionic properties [17]. Detailed studies on decorative hard coatings sputtered from the compounds LaB_6 and ZrB_2 have already been published [18–26]. In this paper we report on the deposition and fundamental properties of decorative coatings sputtered non-reactively from targets with different ratios of LaB_6 and ZrB_2.

2. Experimental details

2.1. Film deposition

Coatings with typical thicknesses of 3 to 4 μm were deposited in a laboratory sputtering system employing non-reactive d.c. magnetron sputtering in argon atmosphere. Commercially available LaB_6 and ZrB_2 disks, all of 150 mm diameter, approximately 6 mm thickness, and 99.5% purity, were employed as targets. Additional targets were manufactured by powder-metallurgical methods within the system LaB_6–ZrB_2 with ZrB_2 contents of 25, 55, and 75 at.%. The substrates employed were austenitic stainless steel (X 5 CrNi 18 10, ground and polished to 1 μm diamond paste), quenched and tempered steel (34 CrNiMo 6, ground and polished to 1 μm diamond paste) and rolled molybdenum sheet. Before deposition they were ultrasonically cleaned in ethanol.

The coating parameters systematically varied in deposition runs included argon pressure, substrate bias voltage and substrate temperature. The substrate-to-target distance was 55 mm. Evacuation of the vacuum chamber was accomplished by a 200 $l\ s^{-1}$ turbomolecular unit backed up by a 16 $m^3\ h^{-1}$ rotary pump down to 2×10^{-2} Pa. During the final stage of the system pump-down the substrates were heated to 400°C using a resistance heater to enhance degassing. The substrate temperature was measured with a NiCr–Ni thermocouple mounted in the back side of the substrate holder. Prior to film deposition the targets were sputter-etched in pure argon for about 2 min at a sputtering power density of 1.7 $W\ cm^{-2}$ target area against a shutter. Immediately thereafter the substrates were sputter-etched for 30 min at an argon pressure of 3 Pa. The d.c. etching voltage was −1500 V. After sputter etching the shutter was opened and the target was operated at a sputtering power density of 2.8 $W\ cm^{-2}$. The deposition rate was measured using a quartz film thickness sensor and monitor at a target-to-substrate distance of 55 mm. For these measurements the bulk density values of the corresponding borides calculated for the given composition were used [27]. After film deposition the samples were cooled down to less than 100°C before the system was vented. Typical deposition parameters are summarized in Table 1.

2.2. Film characterization

The methods employed in analysing the films deposited were the spherical abrasion method, scanning electron microscopy (SEM), electron-probe microanalysis (EPMA), X-ray diffraction (XRD), Vickers microhardness measurements and quantitative colorimetry based on the CIE-$L^*a^*b^*$ method. The spherical abrasion method used for determining the film thickness was conducted on coated quenched and tempered steel substrates with a steel ball of 30 mm diameter and 1 μm diamond paste. For the characterization of the morphology using SEM, coated molybdenum sheets were broken after cooling in liquid nitrogen. EPMA was performed with bulk ZrB_2 and LaB_6 standards [28], the results have been cross-checked and additional standards were obtained by nuclear methods (elastic recoil detection (ERD) and Rutherford backscattering (RBS)). XRD was carried out with coated molybdenum sheets and Cr $K\alpha$ radiation. Vickers microhardness measurements were performed on coated quenched and tempered steel substrates using a conventional microhardness tester at a load of about 98 mN (about 10 p) which was applied for 10 s. For the characterization of the optical behaviour, coated austenitic stainless steel discs were used. Colorimetry was carried out with a conventional colorimeter using a D65 light source and a d/8 geometry, i.e. diffuse illumination and measurement of the reflected light at an angle of 8° with respect to the perpendicular of the surface. Under the CIE-$L^*a^*b^*$ method used, L^* represents the brightness or brilliance of the film, with $L^* = 100$ representing white and $L^* = 0$ representing black; a^* represents proportional red/

Table 1
Deposition parameters used for the targets investigated

ZrB_2 content (at.%)	Sputtering power density ($W\ cm^{-2}$)	Total pressure (Pa)	Bias voltage (−V)	Substrate temperature (°C)
0	2.8	0.95	100	200
25	2.8	0.95	100	250
55	2.8	0.95	100	250
75	2.8	0.95	100	250
100	2.8	1	200	300

green coloration, with $a^* < 0$ representing greenish tones and $a^* > 0$ representing reddish tones; b^* represents proportional blue/yellow coloration, with $b^* < 0$ representing bluish tones and $b^* > 0$ representing yellowish tones [29].

3. Results and discussion

3.1. Deposition rate

The deposition rates measured using the quartz film thickness sensor and monitor showed a maximum for argon pressures in the range of 0.7 to 1.2 Pa (Fig. 1(a)). The decrease observed at low argon pressures is attributed to the increasing plasma impedance, which leads to a decreasing magnetron current and thus to a reduced sputtering rate at constant magnetron power. This reduced sputtering rate at the target due to the decreasing number of impinging argon ions is not balanced by the increased magnetron voltage because of the less than linear dependence of the sputtering yield on the ion energy [30]. The decrease of the growth rate at high argon pressures is due to the increased number of collisions of the sputtered energetic particles with argon atoms resulting in a larger number of thermalized atoms [31,32] with reduced deposition probabilities.

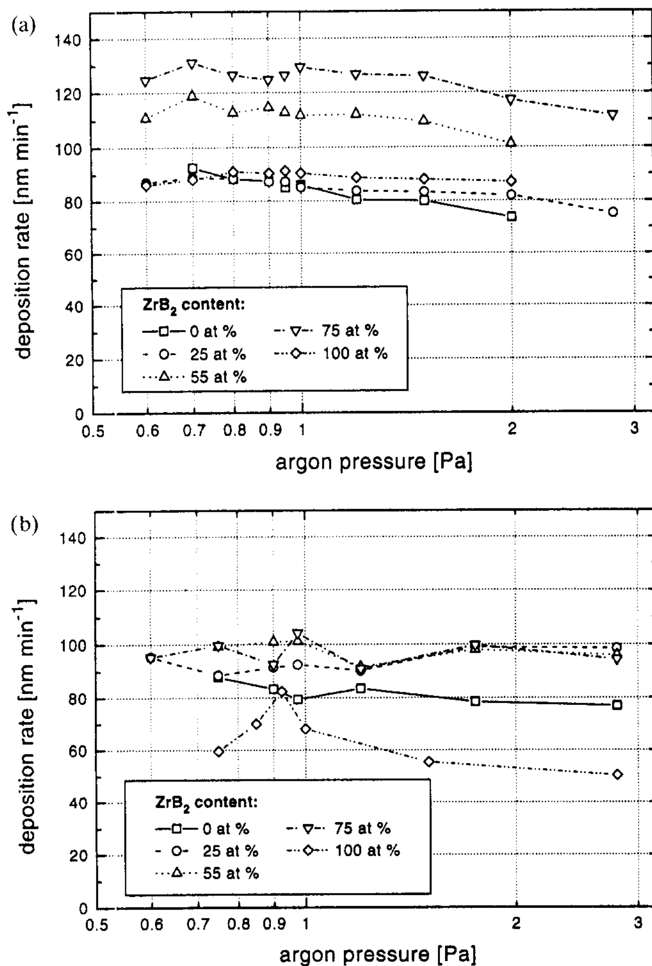

Fig. 1. Deposition rates measured by the quartz film thickness sensor and monitor ((a), grounded and water-cooled sensor) and calculated from the final coating thickness and the corresponding deposition time ((b), deposition parameters see Table 1) of films sputtered from LaB_6–ZrB_2 targets as a function of the argon pressure.

The dependence of the growth rates calculated from the final coating thickness using the spherical abrasion method and the corresponding deposition time on the argon pressure is shown in Fig. 1(b). Despite the fact of the different deposition parameters used for quartz film thickness sensor measurements (grounded and water-cooled sensor) and the spherical abrasion method (biased and heated substrates) an excellent agreement was observed for sputtering from LaB_6-rich targets (ZrB_2 content of 25 at.% or less, compare Fig. 1(a) and 1(b)). The differences between the growth rate measured by the quartz film thickness sensor and the spherical abrasion method for sputtering from those targets alloyed with higher contents of ZrB_2 indicate that the coating density is significantly lower than the bulk density used for the calibration of the sensor. The maximum deviations were observed for those targets alloyed with 55 and 75 at.% ZrB_2. Within the range investigated, no pronounced influence of the deposition parameters bias voltage and substrate temperature on the growth rate was observed.

3.2. Morphology

Fig. 2 shows SEM fracture cross-sections of coatings deposited onto molybdenum substrates. For those coatings sputtered from both the LaB_6 and the ZrB_2 target the deposition conditions showed a distinct influence on film growth. The dense, extremely fine-columnar structure shown in Fig. 2(a) was formed by sputtering from the LaB_6 target using deposition conditions with moderate energetic contribution for film growth. In the complementary growth region, especially at high argon pressures, high bias voltages or low substrate temperatures, the structure of the coatings becomes extremely fine-grained to fracture-amorphous (Fig. 2(b)). Obviously, columnar film growth is not possible with the low energies of sputtered target atoms (at high argon pressures) or high energy ion bombardment (at high bias voltages) [33,34]. Films deposited using the LaB_6–ZrB_2 targets exhibited microstructures that were apparently nearly totally amorphous (Fig. 2(c)). Crystalline film growth seems to be severely inhibited by the incorporation of foreign atoms within films hindering diffusion processes [35].

In the case of sputtering from the LaB_6 target, combinations of extreme deposition parameters, e.g. low argon pressures and high bias voltages, result in

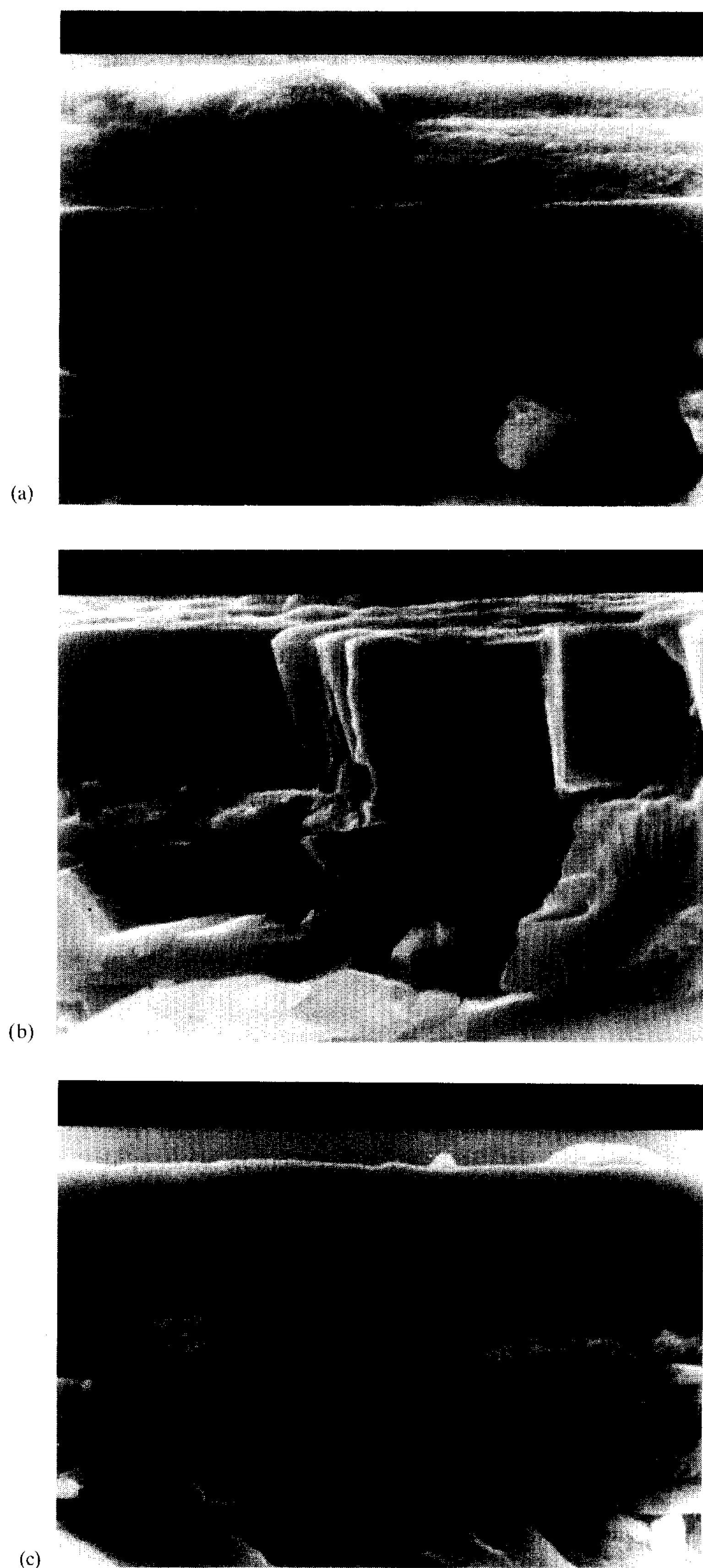

Fig. 2. Cross-sectional SEM micrographs of films deposited onto molybdenum substrates (sputtering power density, 2.8 W cm^{-2}): (a) ZrB_2 target (argon pressure, 2.8 Pa; bias voltage, −200 V; substrate temperature, 200°C); (b) LaB_6 target (argon pressure, 1.2 Pa; bias voltage, −100 V; substrate temperature, 200°C); (c) LaB_6–ZrB_2 target (ZrB_2 content, 75 at.%; argon pressure, 2.8 Pa; bias voltage, −100 V; substrate temperature, 200°C).

the deposition of low adherent coatings. The most crucial deposition parameter with respect to the adhesion was the substrate temperature, with a maximum value for stable coatings of 250°C. This behaviour is obviously due to the differences in the binding character between the coating dominated by covalent boron–boron bonds and the metallic substrate which results in the formation of less pronounced coating–substrate interfaces [35].

3.3. Chemical composition

The dependence of the chemical composition of the coatings on the ZrB_2 content of the target used is plotted in Fig. 3 and compared with the calculated target composition. The maximum deviations between coating and target composition yielded values of up to 4 at.%. In general, in non-reactive sputter processes, stoichiometric deviations of the coating from the target composition are attributable to interactions of the sputtered target atoms with the plasma discharge in the transport phase and at the surface of the growing film, assuming that diffusion processes in the target are inhibited [36]. Therefore, the main reasons for the observed differences between coating and target composition are collisions of sputtered energetic particles with argon atoms as well as preferential resputtering and recoil implantation effects at the film surface. For the atoms involved in the sputtering process, the efficiency of the energy transfer from sputtered target atoms to argon atoms expressed by the energy transfer coefficient [30] shows a maximum for zirconium [19]. These atoms are thus rapidly thermalized [37] and have reduced deposition probabilities. This interpretation is suitable to explain the discrepancy of the zirconium content for deposited coatings and for the corresponding target shown in Fig. 3. Likewise, the boron concentration of the coatings, which is in almost all cases above stoichiometry, may be interpreted by the high mobility of the small boron atoms within the plasma discharge due to the small collision cross-section [8,19].

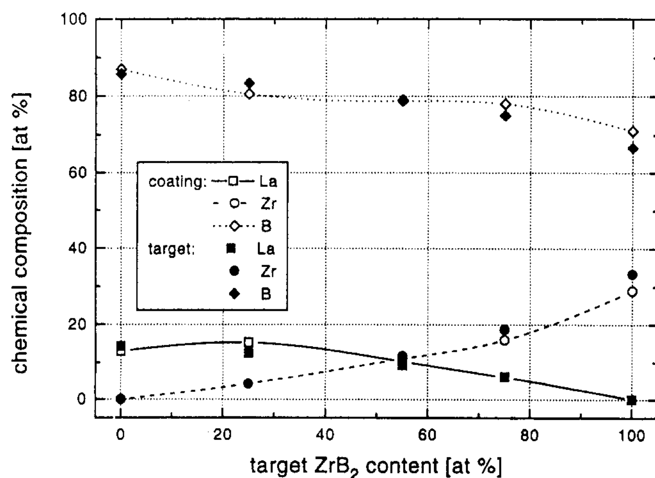

Fig. 3. Chemical composition of coatings sputtered from LaB_6–ZrB_2 targets (deposition parameters see Table 1) with respect to the target composition.

3.4. Crystalline phases

Typical XRD traces of coatings deposited onto molybdenum substrates are shown in Fig. 4. There, the intensity values given in the JCPDS cards [38] for Cu Kα radiation were corrected for the Cr Kα source used in the present work by the Lorentz polarization factor [39].

The XRD spectrum of a coating sputtered from the LaB_6 target shown in Fig. 4(a) indicates the occurrence of the cubic LaB_6 phase having a pronounced (100) texture. With increasing argon pressure, the distinct (100) orientation of the LaB_6 phase estimated by texture coefficients [40,41] becomes even more dominant [8]. Simultaneously, the lattice parameter a of the LaB_6 phase decreases from values of 4.278 Å (corresponding to a distortion of +3.01%) asymptotically to the literature value of bulk LaB_6 ($a = 4.153$ Å [38]). Obviously, the most preferred growth direction of the LaB_6 phase at high argon pressures, i.e. condensation, nucleation, coalescence and crystal growth [42] by highly thermalized particles, is with the (100) planes parallel to the substrate surface resulting in the formation of relatively perfect crystals. The lattice distortions at low argon pressures are assigned to the effect of excess boron (see Fig. 3) [8] and implanted argon atoms [43] or impurities originating from residual gases during the deposition process incorporated interstitially into the LaB_6 lattice. Therefore, and due to the growth under distinctly non-equilibrium conditions without complete coalescence [42], a slight misorientation of the (100) planes of the LaB_6 phase occurs. These results are in good agreement with Kinbara et al. [11] and Nakano et al. [13]. Within the range investigated, no pronounced influence of the deposition parameters bias voltage (0 to −200 V) and substrate temperature (150 to 250°C) on the results of XRD measurements was observed.

The addition of ZrB_2 results in vanishing texture and intensity for the peaks of the LaB_6 phase. For the lowest ZrB_2 contents used (LaB_6–ZrB_2 target with 25 at.% ZrB_2) the LaB_6 phase with a lattice parameter close to the bulk value could be detected from the XRD trace (Fig. 4(b)). With respect to films grown without ZrB_2 addition, a broadening of the peaks was observed (the full width at half maximum (FWHM) values increase from 1.7° to 2.2°). These results may be explained by the formation of films which are partially amorphous and partially containing small crystalline LaB_6 crystals, where excess boron, zirconium, or

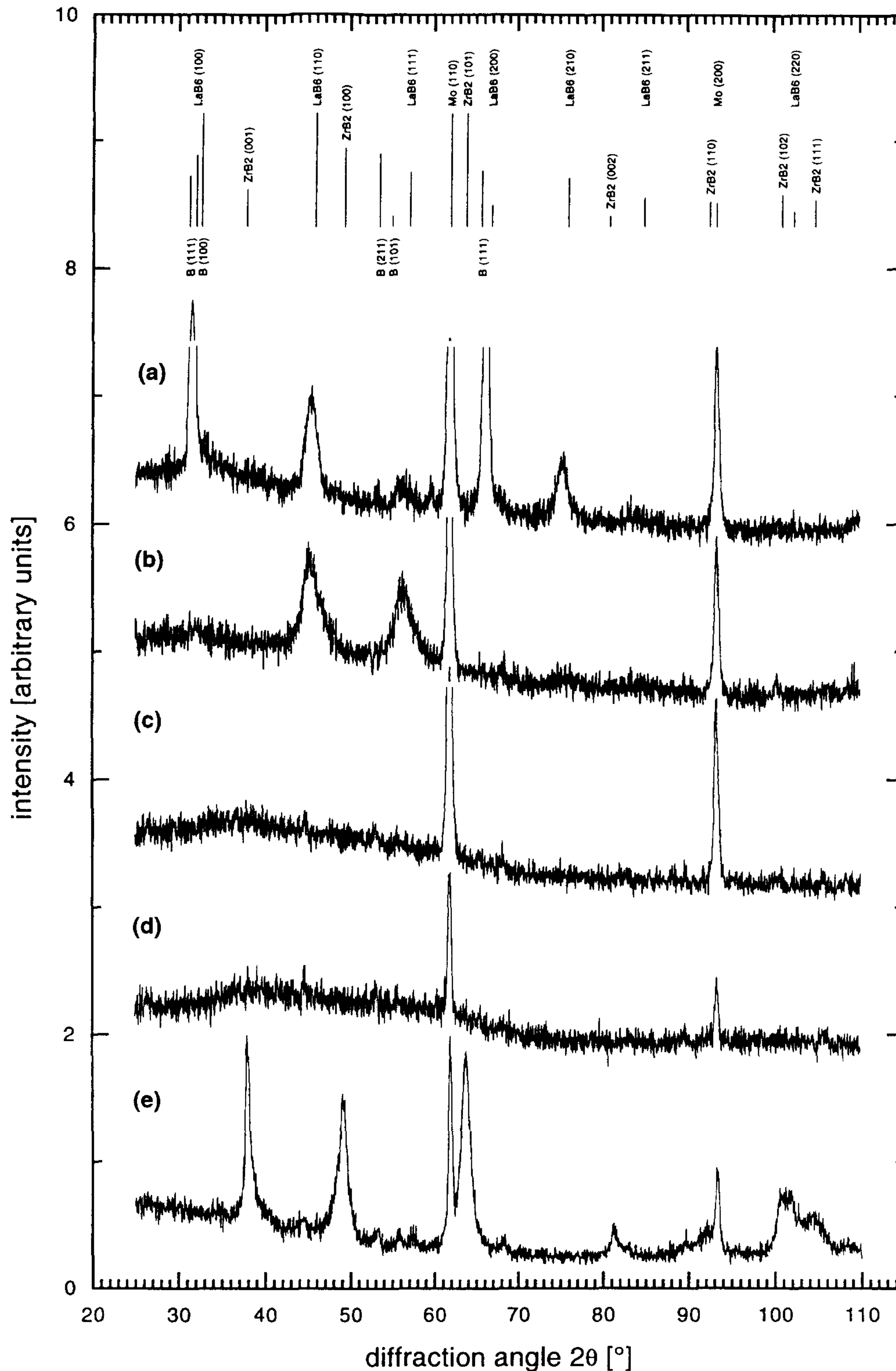

Fig. 4. XRD spectra of films deposited onto molybdenum substrates (sputtering power density, 2.8 W cm^{-2}): (a) LaB_6 target (argon pressure, 0.95 Pa; bias voltage, − 100 V; substrate temperature, 200°C); (b) LaB_6–ZrB_2 target (ZrB_2 content, 25 at.%; argon pressure, 0.95 Pa; bias voltage, − 100 V; substrate temperature, 250°C); (c) LaB_6–ZrB_2 target (ZrB_2 content, 55 at.%; argon pressure, 0.95 Pa; bias voltage, − 100 V; substrate temperature, 250°C); (d) LaB_6–ZrB_2 target (ZrB_2 content, 75 at.%; argon pressure, 0.95 Pa; bias voltage, − 100 V; substrate temperature, 250°C); (e) ZrB_2 target (argon pressure, 1 Pa; bias voltage, − 200 V; substrate temperature, 300°C).

argon atoms causing lattice distortions in crystalline films [43] are incorporated within the amorphous phase. The difference of the preferred growth direction of the LaB_6 phase in ZrB_2-containing films with respect to LaB_6 coatings is interpreted by segregation processes of zirconium and boron atoms at growing LaB_6 nuclei hindering coalescence and growth [42]. The process parameters argon pressure, bias voltage

and substrate temperature showed no pronounced influence on the structure of these films.

Films sputtered from those LaB_6–ZrB_2 targets with ZrB_2 contents of 55 and 75 at.% showed — uninfluenced by the process parameters — broad features in the XRD traces at diffraction angles 2θ of approximately 38° (see Figs. 4(c) and 4(d)) which may be identified as originating from a tendency to order in the sense that atoms are fairly tightly packed together and show a statistical preference for a particular interatomic distance within a boron-rich phase.

In the case of sputtering from ZrB_2 targets, films containing the hexagonal ZrB_2 phase were deposited (Fig. 4(e)). Within the range of the deposition parameters argon pressure (0.75 to 2.8 Pa), bias voltage (0 to − 400 V) and substrate temperature (100 to 400°C) investigated, an almost random orientation of the ZrB_2 phase was observed. Likewise, the lattice parameters of the ZrB_2 phase calculated from the XRD traces vary without pronounced tendency in the range $a = 3.197$ to 3.209 Å and $c = 3.453$ to 3.458 Å. These values correspond to lattice distortions in the a direction of + 0.91 to + 1.30% and parallel to the c axis of − 1.28 to − 2.19% (compared with the literature values of ZrB_2, $a = 3.168$ Å and $c = 3.530$ Å [38]). These distortions are, on the one hand, attributed to the effect of excess boron (see Fig. 3) which may be incorporated interstitially in the ZrB_2 lattice and, on the other hand, to the incorporation of argon atoms [43].

3.5. Microhardness

The dependence of the Vickers microhardness HV 0.01 on the argon pressure is plotted in Fig. 5. For the interpretation of the dependence of the hardness we

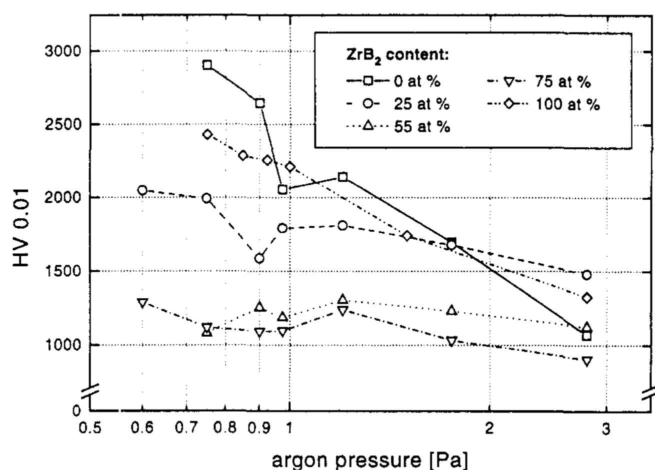

Fig. 5. Dependence of the Vickers microhardness HV 0.01 of coatings sputtered from LaB_6–ZrB_2 targets on the argon pressure (deposition parameters see Table 1).

have to distinguish between crystalline and amorphous films. For coatings with crystalline structure, a distinct decrease of the film hardness was observed with increasing argon pressure. In the case of sputtering from the LaB_6 target, this decrease seems to be in excellent agreement with the distortion of the LaB_6 lattice. In addition, the hardness values obtained at low pressures are in good agreement with the literature values of bulk ZrB_2 (2300 HV 0.05 [27]) and LaB_6 (in the range between 2150 HV 0.1 [27] and 2600 HV 50 [15]). However, surprisingly low hardness values, well below the literature values, are observed for those crystalline coatings deposited at high argon pressures, although in the case of sputtering from the LaB_6 target the B/La atomic ratio is close to stoichiometry (see Fig. 3) and the structure is less distorted. In general, low particle energies and low substrate temperatures favour the formation of low-strength grain boundaries due to incomplete coalescence between growing crystals [42]. In extremely fine-grained to almost fracture-amorphous structures the well-known Hall–Petch relation, valid for comparatively large grain sizes, may therefore be overlapped by the high density of grain boundaries and voids [43]. In addition, internal stresses can be relaxed at open-voided grain boundaries, thus reducing the tendency of the coatings to peel off. The low hardness values obtained at high argon pressures for sputtering from ZrB_2 as well as LaB_6 targets are therefore attributed to the observed extremely fine-grained to fracture-amorphous structure with low-strength grain boundaries of these films. Supporting this interpretation, the influence of the argon pressure on the film hardness decreases with increasing tendency to form amorphous structures.

Corresponding to the insignificant influence of bias voltage and substrate temperature on the film structure, we observed no significant influence of these parameters on the coating hardness.

3.6. Coloration

The results of colorimetric measurements based on the CIE-$L^*a^*b^*$ method are presented in Fig. 6. Films sputtered from those targets alloyed with ZrB_2 exhibited reflective silvery-grey appearances. In colorimetry, this is characterized by relatively high L^* values (in the range between 62 and 74) and chromatic values a^* and b^* close to zero. (Although the positive values for a^* and b^* given in Fig. 6 represent red and yellow colorations respectively, the human eye is obviously not sufficiently sensitive to perceive the resulting orange chroma.) We observed no systematic influence of the argon pressure on the coloration of these films. With chromatic values a^* and b^* of

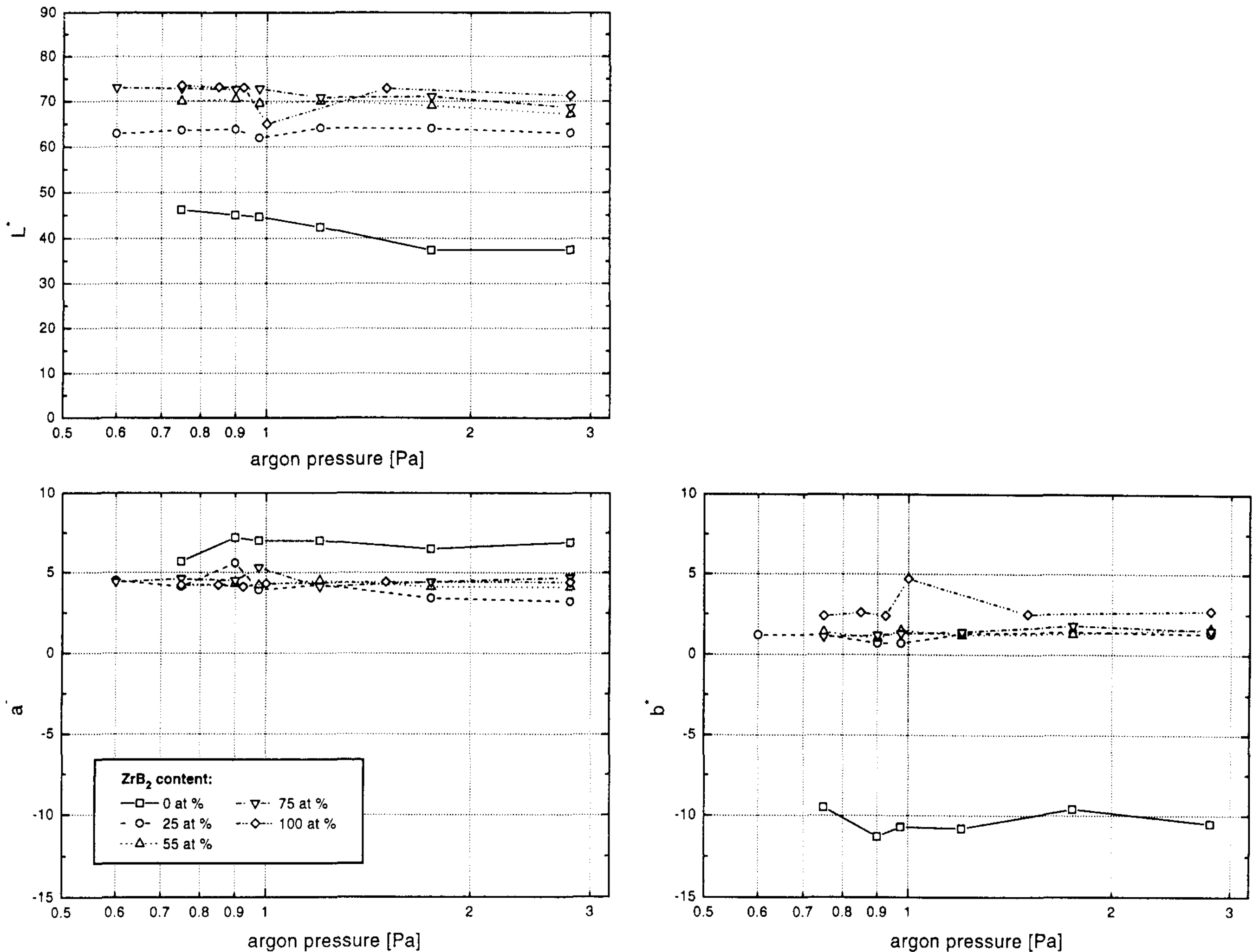

Fig. 6. Dependence of the CIE-$L^*a^*b^*$ values of coatings sputtered from LaB_6–ZrB_2 targets on the argon pressure (deposition parameters see Table 1).

approximately 7 and − 10 respectively, the coloration of coatings sputtered from the LaB_6 target corresponds, rather independently of the argon pressure, to a violet hue. However, owing to the marked decrease of the brilliance value L^* of these coatings with increasing argon pressure, a change in the coloration with respect to human colour perception from violet (argon pressure 1.2 Pa or less) to almost black (argon pressure 1.7 Pa or greater) was observed. In general, the visual impression of bulk LaB_6 with a more distinct red colour component was not achieved by the coatings deposited. Considering the results obtained, there is a good agreement with the work of McKelvy et al. [3] who distinguished the purple stoichiometric LaB_6 from a blue-coloured randomly lanthanum-deficient hexaboride with composition $LaB_{6.13\pm0.03}$. However, it should be noted that structural defects like interstitials, vacancies and impurities, which are typical for coatings grown by low-temperature PVD processes, are expected to reduce the mobility and the relaxation time of free electrons thus affecting the shape of the plasma oscillation edge [44]. This plasma oscillation edge occurring within the visible wavelength spectrum is responsible for the purple-red coloration of the LaB_6 phase [45]. Similar results on LaB_6-based coatings have been published by other groups [46,47]. The marked decrease of the brilliance value L^* with increasing argon pressure has to be attributed to the observed stoichiometric and structural changes.

In the case of coatings deposited by sputtering from the targets alloyed with ZrB_2 the coloration was not influenced significantly by the bias voltage applied. In coatings sputtered from the LaB_6 target we observed a slight shift of the a^* and b^* values from 8 and − 12 (grounded substrates) to 6 and − 10 (bias voltage, −200 V) respectively, whereas the brilliance value was nearly unaffected. Within the range investigated the substrate temperature showed no pronounced influence on the coloration.

3.7. Interrelationships between target composition and film properties

In Fig. 7 the dependence of the Vickers microhardness HV 0.01 and the coloration expressed by the CIE-$L^*a^*b^*$ values is shown as a function of the target ZrB_2 content. There, the plotted data points indicate the average values measured for coatings deposited within the whole parameter range of argon pressure, bias voltage and substrate temperature investigated, whereas the error bars give the maximum and minimum values obtained. The Vickers microhardness of coatings deposited from both the pure LaB_6 and ZrB_2 targets yielded values similar to those reported by Ordan'yan et al. [16] for bulk LaB_6 and ZrB_2 samples (see Fig. 7(a)). However, in the region of partially amorphous or amorphous film growth, i.e. in the two-phase region of the quasi-binary section LaB_6–ZrB_2, a marked difference of the hardness values for bulk samples and coatings was observed. Hardness values as low as those plotted in Fig. 7(a) have been reported by other authors [35,48] and are a result of low-temperature film growth with energetic contributions not sufficient for long-distance diffusion processes needed for phase separation. Corresponding to the tendency to form amorphous films within the two-phase region of the quasi-binary section LaB_6–ZrB_2, the violet coloration of LaB_6 coatings is not maintained if the target is alloyed with the ZrB_2 contents used in this investigation (see Fig. 7(b)).

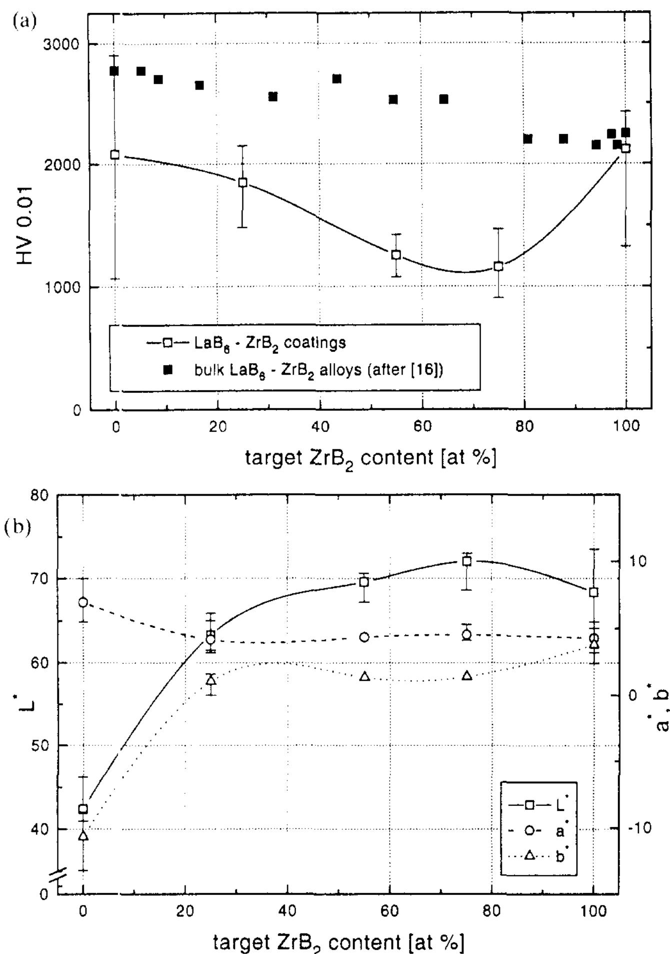

Fig. 7. Dependence of (a) the Vickers microhardness HV 0.01 and (b) CIE-$L^*a^*b^*$ values of coatings sputtered from LaB_6–ZrB_2 targets on the target ZrB_2 content (deposition parameters see Table 1).

4. Conclusions

Based on the characterization work done on decorative coatings sputtered from targets within the quasi-binary system LaB_6–ZrB_2 we draw the following conclusions. On the one hand, alloying with ZrB_2 is well suited to overcome some mechanical drawbacks of LaB_6-based coatings due to stress relaxation. On the other hand, the ZrB_2 contents investigated result in the formation of partially amorphous or amorphous film structures within the two-phase region of the eutectic LaB_6–ZrB_2 system. Thus, the optical properties of these alloyed films are no longer related to those of the LaB_6 phase. Looking ahead, although we have not succeeded optimizing both coloration and mechanical properties of ZrB_2-alloyed LaB_6-based coatings, complex two- or multi-phase coatings have a substantial potential for certain applications. Further work to improve LaB_6-based coatings using a cosputtering technique is currently underway [49].

Acknowledgements

The authors are grateful to G. Hawranek (Institut für Metallkunde und Werkstoffprüfung, Montanuniversität Leoben) for his help in SEM characterization of the coatings. We would also like to thank Dr. P. Rödhammer and Dipl.-Ing. E. Garber (Metallwerk Plansee, Reutte) for supplying the molybdenum sheets and for the assistance in preparing the boride powders, Dr. H. Knoch (Elektroschmelzwerk Kempten) for manufacturing the LaB_6–ZrB_2 targets and Dr. H. Baumann (Institut für Kernphysik, Universität Frankfurt) for RBS and ERD analysis.

References

[1] J.M. Lafferty, *J. Appl. Phys.*, *22* (1951) 299.
[2] T. Niemyski and E. Kierzek-Pecold, *J. Cryst. Growth*, *3–4* (1968) 162.
[3] M.J. McKelvy, L. Eyring and E.K. Storms, *J. Phys. Chem.*, *88* (1984) 1785.
[4] S.J. Mroczkowski, *J. Vac. Sci. Technol. A*, *9* (3) (1991) 586.
[5] A. Yutani, A. Kobayashi and A. Kinbara, *Appl. Surf. Sci.*, *70–71* (1993) 737.

[6] W. Waldhauser, C. Mitterer, J. Laimer and H. Störi, *Surf. Coat. Technol., 74–75* (1995) 890.

[7] W. Schintlmeister and O. Pacher, *J. Vac. Sci. Technol., 4* (1975) 743.

[8] C. Mitterer, J. Komenda-Stallmaier, P. Losbichler, P. Schmölz and H. Störi, *Surf. Coat. Technol., 74–75* (1995) 1020.

[9] L.J. Favreau, *Rev. Sci. Instrum., 36* (1965) 856.

[10] R.S. Khairnar, P.W. Mahajan, D.S. Joag, A.S. Nigavekar and P.L. Kanitkar, *J. Vac. Sci. Technol. A, 3* (2) (1985) 398.

[11] A. Kinbara, T. Nakano, A. Kobayashi, S. Baba and T. Kajiwara, *Appl. Surf. Sci., 70–71* (1993) 742.

[12] T. Kajiwara, T. Urakabe, K. Sano, K. Fukuyama, K. Watanabe, S. Baba, T. Nakano and A. Kinbara, *Vacuum, 41* (4–6) (1991) 1224.

[13] T. Nakano, S. Baba, A. Kobayashi, A. Kinbara, T. Kajiwara and K. Watanabe, *J. Vac. Sci. Technol. A, 9* (3) (1991) 547.

[14] J. Etourneau, J.-P. Mercurio and P. Hagenmuller, in V.I. Matkovic (ed.), *Boron and Refractory Borides*, Springer, Berlin, 1977, p. 115.

[15] F. Binder, *Radex-Rundschau, 1* (1977) 52.

[16] S.S. Ordan'yan, Yu.B. Paderno, I.K. Khoroshilova, E.E. Nikolaeva and E.V. Maksimova, *Sov. Powder Metall. Met. Ceram., 22* (1983) 956.

[17] T.E. Zapadaeva, E.E. Nikolaeva, S.S. Ordan'yan and V.A. Petrov, *Sov. Powder Metall. Met. Ceram., 26* (1987) 581.

[18] J. Stallmaier, C. Mitterer and J. Barounig, *Le Vide, les Couches Minces, 261* (1992) 265.

[19] C. Mitterer, J. Komenda-Stallmaier, P. Losbichler, P. Schmölz, W.S.M. Werner and H. Störi, *Vacuum, 46* (11) (1995) 1281.

[20] E. Brandstetter, C. Mitterer and R. Ebner, *Thin Solid Films, 201* (1991) 123.

[21] C. Mitterer, A. Übleis and R. Ebner, *Mater. Sci. Eng. A, 140* (1991) 670.

[22] C. Mitterer, P. Losbichler, W.S.M. Werner, H. Störi and J. Barounig, *Surf. Coat. Technol., 54–55* (1992) 329.

[23] A. Übleis, C. Mitterer and R. Ebner, *Surf. Coat. Technol., 60* (1993) 571.

[24] C. Mitterer, P. Schmölz and H. Störi, *Metall (Berlin), 48* (3) (1994) 202.

[25] M. Ürgen, A.F. Çakir, O.L. Eryilmaz and C. Mitterer, *Surf. Coat. Technol., 71* (1995) 60.

[26] M. Ürgen, A.F. Çakir, O.L. Eryilmaz and C. Mitterer, *Prakt. Metall., 32* (1995) 126.

[27] F. Binder, *Radex-Rundschau, 4* (1975) 531.

[28] G.F. Bastin and H.J.M. Heijligers, *J. Microsc. Spectrosc. Electron., 11* (1986) 215.

[29] R.M. German, M.M. Guzovski and D.C. Wright, *J. Met., 3* (1980) 20.

[30] J.A. Thornton, in R.F. Bunshah (ed.), *Deposition Technologies for Films and Coatings*, Noyes Publications, Park Ridge, NJ, 1982, pp. 170–243.

[31] R.S. Uppadhye and E.J. Hsieh, *J. Vac. Sci. Technol. A, 10* (3) (1990) 1348.

[32] R. Elsing, *Surf. Coat. Technol., 49* (1991) 132.

[33] G. Håkansson, J.-E. Sundgren, D. McIntyre and J.E. Greene, *Thin Solid Films, 153* (1987) 55.

[34] I. Petrov, L. Hultman, U. Helmersson, J.-E. Sundgren and J.E. Greene, *Thin Solid Films, 169* (1989) 299.

[35] H. Holleck, *Metall (Berlin), 43* (7) (1989) 614.

[36] G. Betz, M. Opitz and P. Braun, *Nucl. Instrum. Methods, 182–183* (1981) 63.

[37] I. Petrov, I. Ivanov, V. Orlinov and J.-E. Sundgren, *J. Vac. Sci. Technol. A, 10* (3) (1990) 1348.

[38] *Powder Diffraction File*, Joint Committee on Powder Diffraction Standards, International Center for Diffraction Data, Swarthmore, PA, Cards 6-0401, 34-423.

[39] B.D. Cullity, *Elements of X-Ray Diffraction*, Addison-Wesley, Reading, MA, 1978, p. 131.

[40] A.J. Perry, *Thin Solid Films, 138* (1986) 73.

[41] A.J. Perry, M. Georgson and W.D. Sproul, *Thin Solid Films, 157* (1988) 255.

[42] P.B. Barna, in L. Eckertová and T. Růžička (eds.), *Diagnostics and Applications of Thin Films*, Institute of Physics, Bristol, 1992, p. 295.

[43] J.-E. Sundgren, *Thin Solid Films, 128* (1985) 21.

[44] R.E. Hummel, *Electronic Properties of Materials*, Springer, Berlin, 1993.

[45] V.I. Bessaraba, L.A. Ivanchenko and Yu.B. Paderno, *J. Less-Common Met., 67* (1979) 505.

[46] S. Winsztal, H. Majewska-Minor, M. Wiśniewska and T. Niemyski, *Mater. Res. Bull., 8* (1973) 1329.

[47] K.R. Peschmann, J.T. Calow and K.G. Knauff, *J. Appl. Phys., 44* (5) (1973) 2252.

[48] H. Holleck and M. Lahres, *Mater. Sci. Eng. A, 140* (1991) 609.

[49] V.-H. Derflinger, W. Waldhauser, C. Mitterer, P. Schmölz and